Fundamentals and Applications of Mo and Nb Alloying in High Performance Steels – Volume 2
Edited by Hardy Mohrbacher
CBMM, IMOA and TMS, 2015

THE SYNERGISTIC EFFECT OF NIOBIUM-MOLYBDENUM ADDITIONS ON THE MICROSTRUCTURE OF LOW-CARBON BAINITIC STEEL

B.M. Huang[1], J.R. Yang[1] and C.Y. Huang[2]

[1]Department of Materials Science and Engineering, National Taiwan University, Taipei, Taiwan, ROC
[2]Steel & Aluminum Research & Development Department, China Steel Corporation, Kaohsiung, Taiwan, ROC

Keywords: Niobium, Molybdenum, Bainitic Steels, Accelerated Cooling, Tempering, SEM, TEM, Precipitation, EBSD, Mechanical Properties, Hardness

Abstract

The main purpose of this work was to elucidate the effect of Mo additions on the development of microstructure in hot rolled low-C Nb-containing bainitic steels. Three experimental steels have been investigated; they had the same base composition of 0.05%C-1.7%Mn-0.08%Nb (wt.%); one had no Mo addition and the other two contained 0.1 wt.% and 0.3 wt.%Mo, respectively. The steel strips were manufactured by a combined process of controlled rolling and accelerated cooling. After finish rolling at 900 °C, the steels were treated by accelerated cooling to 650 °C, 550 °C and 450 °C respectively, and immediately held at that temperature for 10 minutes so that the effects on coiling at the different temperatures could be simulated.

Tempering treatments at 600 °C for different times ranging from 0.5 to 8 hours were performed to investigate the tempered structures and related properties. Through a series of Optical Microscopy (OM), SEM and TEM examinations and mechanical testing, the results indicated that the steel with the addition of 0.3 wt.%Mo had the advantage of producing a high volume fraction of granular bainite, which gained significant benefits from precipitation hardening whilst achieving increased elongation after the tempering treatment.

Introduction

In accordance with the demand for reduced fuel consumption and CO_2 emissions in the automotive and construction industries, the development of advanced high strength steels has been progressing. Weight reduction can be achieved through the use of higher strength steels, however, formability and weldability are also vital factors in the majority of industrial applications. In addition, sufficient toughness is a prerequisite to ensure structural integrity. Ideally, a low-C bainitic microstructure offers an excellent combination of good toughness, strength and weldability [1-3]. The development of low-C bainitic steels originates from the concept that an extremely low C concentration can reduce or eliminate the interplate cementite in a bainitic ferrite matrix and hence the steel's toughness can be further improved.

Under a combined process of controlled-rolling and accelerated-cooling, the production of a high quantity of a bainitic microstructure in low-C low-alloy steels can be achieved. This processing procedure highly depends on the microalloying of Nb [2-5], since Nb has a significant effect on the retardation of recovery and recrystallization of austenite during hot rolling. With this alloy design, the recrystallization stop temperature can be shifted to higher levels. The temperature at which the rolling operation finishes is critical in the sense that it should leave the final austenite grains in an unrecrystallized pancake shape. This ensures a further degree of microstructure refinement from the bainite transformation.

In low-C bainitic steels, bainitic microstructures possess a much finer effective grain size (a platelet thickness of about 0.5 μm) and a higher dislocation density (about 1.7×10^{14} m^{-2}) [1]; relative to conventional ferrite/pearlitic steels. With higher amounts of bainite, higher strengths can be achieved due to the fine size of the bainite platelets and the high dislocation density. The characteristic structures do not impair toughness since the finer grain size compensates for the deterioration in toughness caused by dislocation hardening. The low-C bainitic microstructure achieves the required properties of increased strength without an adverse effect on toughness.

It has been asserted [6-8] that Nb-Mo containing HSLA steels produce a bainitic structure and possess excellent strength-retention characteristics at high temperatures (up to 600 °C or 700 °C), in comparison to conventional HSLA steels containing Nb and V. This finding strongly indicates that the combined addition of Nb and Mo plays an important role in significantly improving the strength of the HSLA steels at both room temperature and high temperatures (up to 700 °C). The information concerning the nano-structural characterization is absolutely essential for alloy design. However, the microstructural evolution associated with a consequent strengthening mechanism has not been studied systematically in previous research. The purpose of this study is to gain an improved and detailed appreciation of the low-C bainite substructure and to evaluate its characteristics and effect on the mechanical properties. The synergistic effect of Nb-Mo additions on the formation of low-C bainite is evaluated. The work also focuses on the tempering effect on the developed low-C bainitic strips in order to evaluate the corresponding secondary hardening.

Experimental Procedure

The investigation involved three different steels. These three experimental steels were prepared by vacuum melting, and then cast into 100 kg slabs with a thickness of 160 mm. The chemical compositions of the steels are listed in Table I. The Nb-containing (0.05%C-1.7%Mn-0.08%Nb (wt.%)) steel was chosen as the reference steel. To determine the synergistic effects of Nb-Mo additions, the other two steels had the same base composition (0.05%C-1.7%Mn-0.08%Nb (wt.%)) and were alloyed with 0.1 and 0.3 wt.%Mo separately. The reference steel was designated as Steel Nb, while the 0.1 and 0.3 wt.%Mo containing steels were designated as Steel Nb-Mo and Steel Nb-3Mo respectively. The steels also contained 0.016 wt.%Ti in order to fix the N by producing stable TN particles. It was calculated that the Ti concentration (wt.%) should be about 3.4 times that of N if the latter was to be fixed [1]. The steel strip samples were produced from the slabs by a combined process of controlled-rolling and accelerated-cooling. A schematic diagram of the whole process is presented in Figure 1. During rolling in the austenite phase a portion of the Nb would precipitate as NbC due to strain-induced precipitation. The NbC

and TiN precipitates serve to prevent austenite grain growth during controlled-rolling operations, which is an additional, essential feature of these steels. A higher portion of Nb (estimated to be as high as 0.04 wt.%) is designed to remain in austenite solid solution. The unrecrystallized, pancake-shaped austenite with a high "soluble" Nb content promotes bainite formation during the accelerated cooling. The major task in the project was to investigate whether secondary hardening occurs in the bainite within these three experimental steels after tempering treatments.

Table I. The Composition of Hot Rolled Strip (wt.%)

Strip	C	Mn	Si	Nb	Mo
Nb	0.05	1.7	0.2	0.08	—
Nb-Mo	0.05	1.7	0.2	0.08	0.1
Nb-3Mo	0.05	1.7	0.2	0.08	0.3

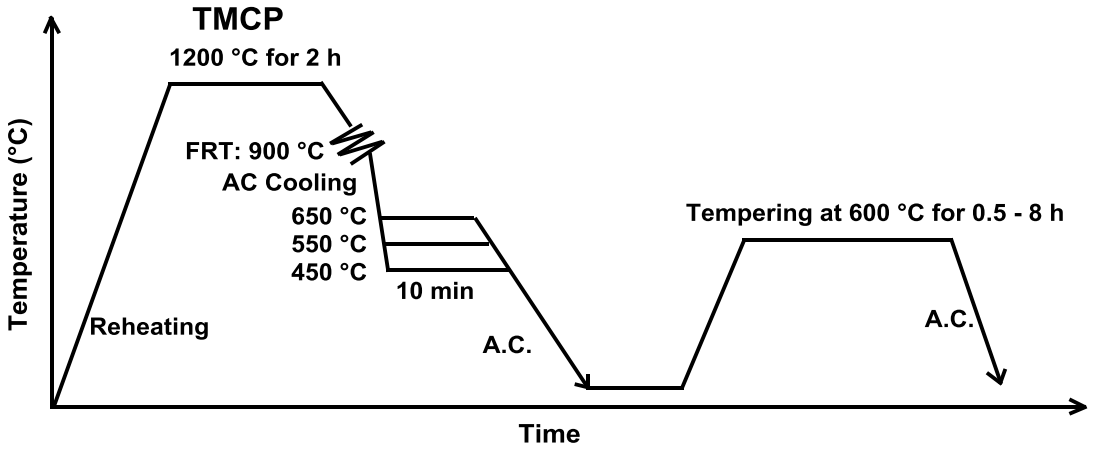

Figure 1. Schematic diagram of the thermomechanical process (with accelerated-cooling and isothermal holding) and the tempering process.

The slabs were heated to 1200 °C and held for 2 hours before rough rolling, which began at 1050 °C. During the course of rolling, the temperatures were measured by an optical pyrometer. The rolling reduction per pass was about 20% and the finish-rolling thickness was 5 mm. After finish-rolling at 900 °C, the strips were accelerated cooled to 650 °C, 550 °C and 450 °C respectively, then held at this temperature for 10 minutes, and finally cooled to room temperature by air cooling (A.C.). Depending on the holding temperatures (650, 550 and 450 °C), these three different steels were designated as Nb-650, Nb-Mo-650, Nb-3Mo-650; Nb-550, Nb-Mo-550, Nb-3Mo-550, Nb-450, Nb-Mo-450 and Nb-3Mo-450, accordingly. The samples were then tempered at 600 °C for different time periods (0.5, 1, 2, 4, and 8 hours) in order to investigate the effect of tempering the bainite.

The specimens for optical metallography (OM) and scanning electron microscopy (SEM), which were cut from the hot rolled strip samples, were mechanically ground with various SiC papers. The specimens were polished and then etched with 3% nitric acid. The Vickers hardness test was conducted under the condition of 1 kg load and 5 seconds loading time. Transmission electron microscopy (TEM) specimens were prepared by cutting discs from the strip samples (along the cross-section), thinning mechanically to 0.06 mm and then twin jet electropolishing to perforation using a mixture of 5% perchloric acid, 20% glycerol, and 75% ethanol at -2 °C, at a potential of 35 V. The specimens were examined on a Tecnai F30 field emission gun scanning transmission electron microscope equipped with an energy dispersive X-ray (EDX) spectrometer. The specimens for the Tecnai Nova 450 SEM-EBSD (electron backscatter diffraction) were prepared by the same method as the TEM thin foils, but without perforation. Orientation mapping for the EBSD data was performed with a 200 nm step size. Bruker-CrystAlign software was used for orientation measurement and analysis.

Results and Discussion

SEM examination of strip samples Nb-450, Nb-Mo-450, Nb-550 and Nb-Mo-550 are presented in Figure 2. They show that the second-phase particles are dispersed among coarse ferrite plates, which appear to have a granular morphology (ie. conventionally so-called granular bainite). In Figure 3, under SEM examination a striking feature of Strip Nb-3Mo is that the prior austenite grain boundaries are aligned along the rolling direction and appear as straight markings. This is because the finish-rolling leaves the final austenite in an unrecrystallized pancake shape. However, parts of the prior austenite grain boundaries become unclear as they are decorated by fine grains of allotriomorphic ferrite (as shown in Figure 3). Optical micrographs, as shown in Figure 4, show the microstructures of strip samples Nb-450, Nb-Mo-450 and Nb-3Mo-450. Microstructural characterization focused on these three samples as they consisted of high quantities of granular bainite. It is absolutely vital to have the quantitative volume fractions of granular bainite, M/A constituents etc., so that the structure-property relationships can be evaluated. As will be seen later in this section, quantitative metallography assessed by using SEM-EBSD is utilized in this work. The volume percentages (vol.%) of different phases in the three hot-rolled strip samples are listed in Table II. It is apparent that the addition of Mo can improve the hardenability with respect to bainitic transformation. The detailed structures of the samples have been studied by TEM. The representative TEM images for allotriomorphic ferrite and granular bainite are presented in Figure 5. Figure 5(a) shows that the allotriomorphic ferrite possesses an equi-axed morphology, which does not contain any subgrain structure; the strain-induced Nb carbides can be seen in the allotriomorphic ferrite grains. Figure 5(b) displays the typical substructural features of granular bainite, which clearly indicates that the coarse ferrite plates referred to as granular bainite do not really exist. In fact, the TEM micrograph clearly indicates that the coarse plate of granular bainite is composed of parallel fine elongated platelets, with a thickness of about 0.5 μm. The TEM results are very similar to those reported elsewhere [9-14]. The morphology of fine elongated platelet shapes is directly related to the displacive transformation [15]. The parallel fine elongated platelets have a similar orientation and form a sheaf morphology, which is not different from ordinary bainite. The peculiar feature of granular bainite is the lack of the austenite thin films and carbides within the bainitic ferrite because of the low C content. The formation of second phases (M/A constituents) results from the C that is partitioned from the bainitic ferrite stabilizing the residual austenite, so that the final

microstructure contains both retained austenite and some high-C martensite. The microstructures of the second phases depend on the degree of C enrichment.

Table II. The Volume Fraction of Phases in the Three Hot Rolled Strip Samples
(F: allotriomorphic ferrite, G.B.: granular bainite, M/A: martensite/austenite constituent, D.P.: degenerate pearlite, vol.%)

Phases/Strip	Nb-450	Nb-Mo-450	Nb-3Mo-450
F	25	14	8
G.B.	63	66	79
M/A	9	19	2
D.P.	3	1	11

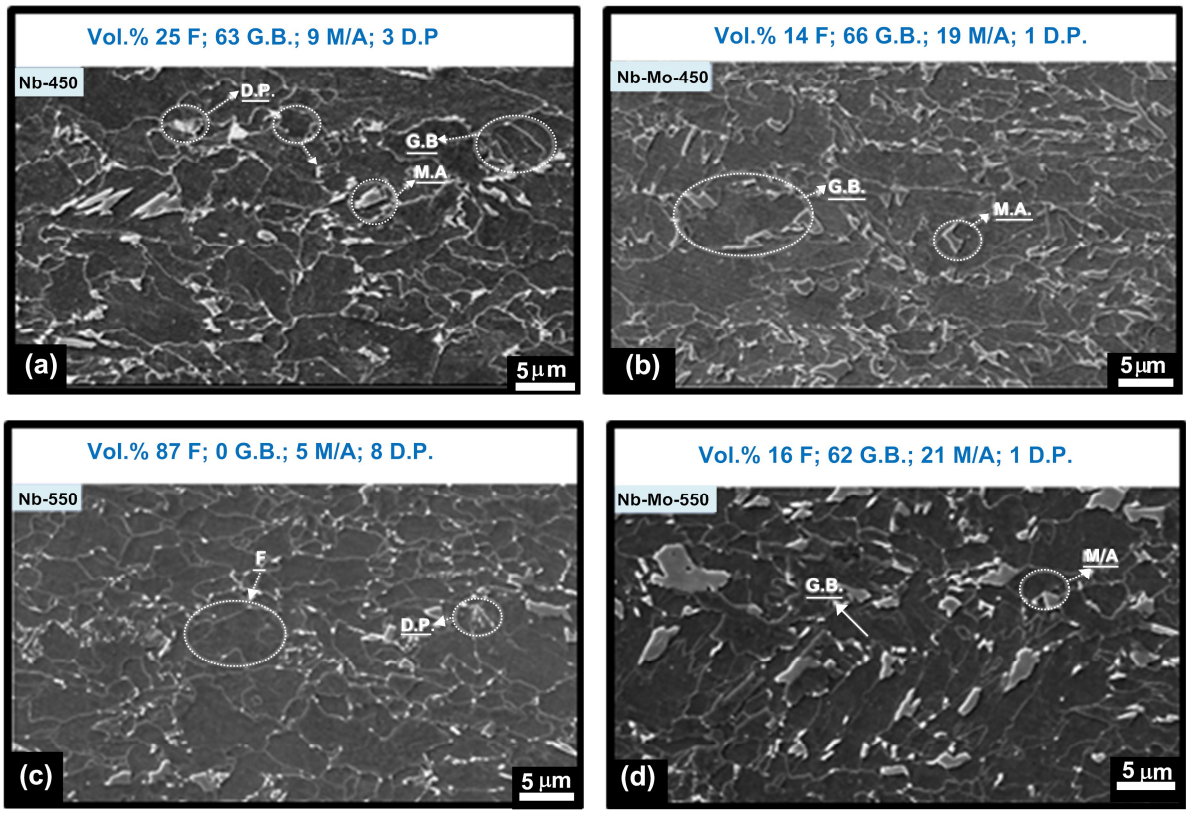

Figure 2. SEM micrographs illustrating all phases including granular bainite (G.B.), allotriomorphic ferrite (F), martensite/austenite constituents (M/A), and degenerate pearlite (D.P.) in; (a) Nb-450, (b) Nb-Mo-450, (c) Nb-550 and (d) Nb-Mo-550.

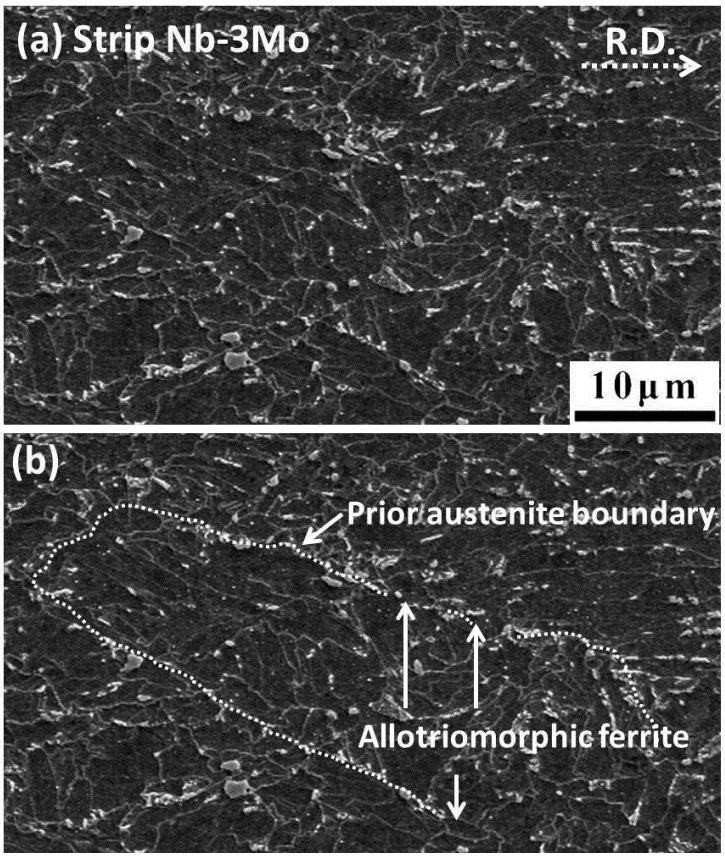

Figure 3. (a) SEM image showing the microstructure of Strip Nb-3Mo, (R.D.: rolling direction), (b) the prior austenite grain boundary depicted with dashed lines and arrowed lines indicating the distribution of allotriomorphic ferrite along grain boundary in (a).

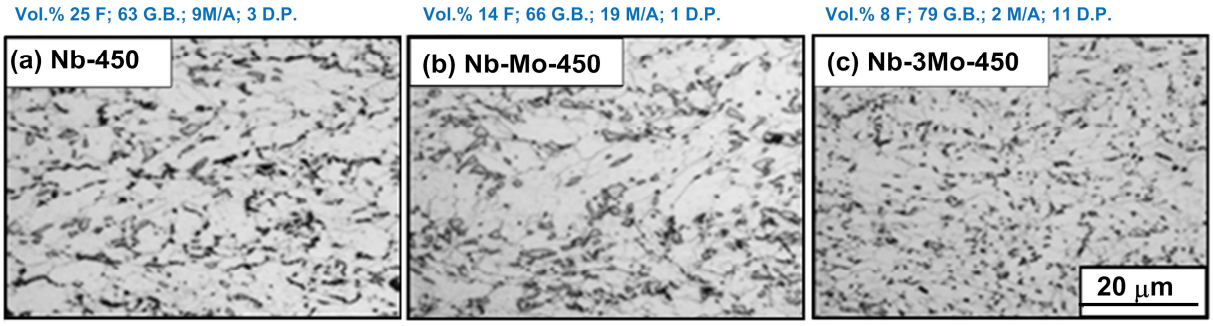

Figure 4. OM micrographs showing the microstructures of; (a) Nb-450, (b) Nb-Mo-450, (c) Nb-3Mo-450. Granular bainite (G.B.), allotriomorphic ferrite (F), martensite/austenite constituents (M/A), and degenerate pearlite (D.P.).

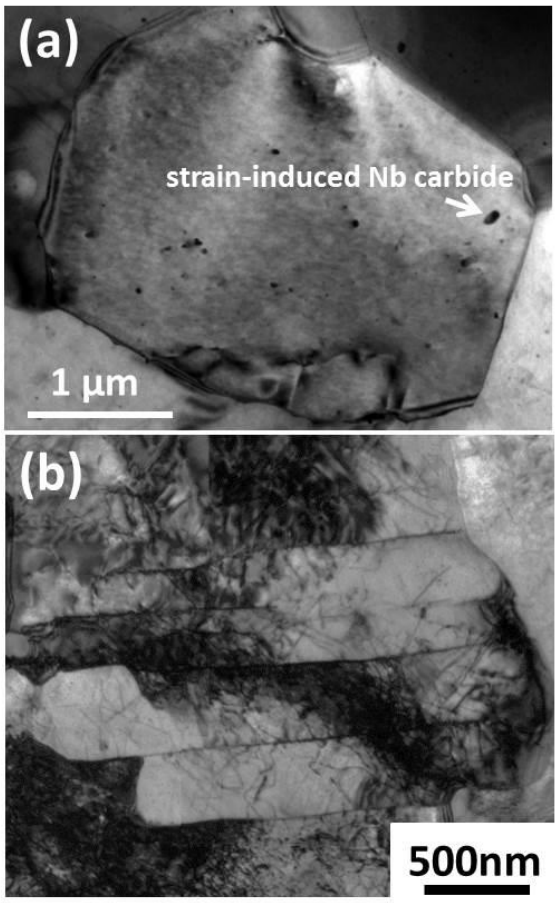

Figure 5. TEM micrographs showing; (a) allotriomorphic ferrite and (b) granular bainite in Nb-Mo-450 strip.

Although TEM can be used to observe the morphology of granular bainite and determine the sub-unit ferrite platelet boundaries, it has difficulty in assessing the volume fraction of granular bainite in the steel strips, with varying Mo additions, due to the limits of the analyzed area. In this work a SEM-EBSD technique has been utilized to obtain crystallographic data for quantitative metallography. The orientation relationship between a pair of like crystals, the crystallographic bases of which are defined from a common origin, can be presented using a rotation matrix. From the rotation matrix, a corresponding axis/angle pair can be derived. This infers that, if one of the crystals is rigidly rotated about the specified axis which passes through the original, through a right-handed angle of rotation h, its orientation coincides with that of the other. For each pair of ferrite (body-centered cubic, bcc) crystals, there are 24 crystallographically equivalent descriptions in terms of axis angle pairs or rotation matrices [16]. In the present EBSD work, the equivalent axis angle pair with the smallest angle of rotation was chosen for each pair of adjacent ferrite grains in order to interpret the data clearly.

The orientation micrograph in Figure 6(a) is obtained from EBSD imaging of the granular bainite in strip sample Nb-450; the distribution of colors in the overall microstructure depends on the crystal orientation. The image is associated with the contrasts in brightness for corresponding Kikuchi patterns generated from all points on the analyzed sample. The image quality of granular bainite is a matter of concern because the high dislocation densities in bainite can reduce the quality of Kikuchi patterns and cause misleading representations of the misorientation angle. In order to elucidate this, the regions marked with A and B in Figure 6(a) have been examined. The corresponding Kikuchi patterns for point A and point B, in Figures 6(d) and 6(e), are clearly shown with an image quality of over 0.6, which indicates that the dislocation density in granular bainite does not have a serious effect on the EBSD imaging. In the present study, the detection of the misorientation angle is significant for microstructural characterization and needs to be elucidated clearly. In the cubic system, there are 24 axis angle pairs for a given adjacent ferrite sub-unit. The misorientation angle can be obtained after the axis angle pair was calculated. The misorientation angle profile versus the scanned distance (as shown in 6(b)) is obtained by using CrystAlign software of Bruker Corp. It indicates that Point A (A matrix) has a relative 2.99º misorientation angle to Point B (B matrix). The Euler angles of Points A and B are (324º 21º 12º) and (320º 19º 14º) respectively, relative to the coordination of the sample (S). They can be derived to the following rotation matrixes relative to the coordination of the sample.

Coordinate transformation matrix for S to A $(A\ J\ S) = \begin{bmatrix} 0.905 & \overline{0.418} & 0.075 \\ 0.369 & 0.861 & 0.351 \\ \overline{0.211} & \overline{0.290} & 0.934 \end{bmatrix}$

Coordinate transformation matrix for S to B $(B\ J\ S) = \begin{bmatrix} 0.890 & \overline{0.448} & 0.079 \\ 0.404 & 0.858 & 0.316 \\ \overline{0.209} & \overline{0.249} & 0.946 \end{bmatrix}$

The coordinate transformation matrix for B to A can be derived as follows.

$$(A\ J\ B) = \begin{bmatrix} 0.999 & 0.037 & 0.013 \\ \overline{0.037} & 0.999 & 0.035 \\ \overline{0.011} & \overline{0.035} & 0.999 \end{bmatrix}$$

The detailed notation of coordinate transformation matrices can be referred to the relevant worked example in [16]. From the coordinate transformation matrix (A J B), 24 equivalent axis-angle pairs can be obtained as shown in Table III. The axis angle pair with the smallest angle of rotation, [0.9971 -0.2312 0.7082]/2.99°, is listed first. It is noted that the smallest angle has been chosen for the general interpretation of the misorientation of the adjacent structures in the EBSD image. In Figure 6(a), the coarse plate region (marked by A-B) is recognized as granular bainite because of the low-angle misorientation boundary of sub-unit platelets; the corresponding plot for misorientation angle versus the detected distance is shown in Figure 6(b). On the other hand, the region marked by C-D in Figure 6(a) is recognized as a ferrite microstructure since no subgrain boundary can be detected (as shown in Figure 6(c)). EBSD measurements were carried out to provide information regarding the density distribution for the misorientation of the boundaries in the microstructure for samples Nb-450, Nb-Mo-450 and Nb-3Mo-450. The density distributions of grain boundary misorientation angles for these strips (with a scanned area of 100 x 100 μm in each sample) are displayed in Figure 7; it is clearly demonstrated that two peaks (with highest frequency) are located around 0-10° and 50-60°. The result is consistent with that reported in the previous work for a high quantity of bainitic structure [17]. In this work, the volume percentages of ferrite and granular bainite were measured from EBSD images, and the volume percentages of M/A phases and degenerate pearlite in second phases were estimated from SEM images. The combined data from SEM and EBSD images were used to estimate the volume percentages of phases and the results are shown in Table II. They indicate that the addition of 0.1 wt.%Mo obviously retards the allotriomorphic ferrite formation but only slightly promotes the granular bainite formation. Rather, there is a significant increase in M/A constituent instead. They also show that the addition of 0.3 wt.%Mo greatly suppresses allotriomorphic ferrite formation but significantly promotes granular bainite transformation and refines the whole microstructure.

Table III. The 24 Axis-Angle Pairs for Adjacent Grains A and B

No.	**Axis**			**Angle (^{o})**
1	0.6671	-0.2312	0.7082	2.99
2	-0.5216	-0.5769	-0.6286	119.8
3	0.523	0.6296	0.5745	120.5
4	-0.0015	-0.7052	0.709	172.5
5	0.7379	-0.674	0.0354	176.4
6	-0.7395	-0.0301	0.6725	176.1
7	-0.9957	0.0021	-0.0926	89.9
8	-0.0406	0.9981	-0.0457	95.5
9	-0.674	-0.738	-0.0316	175.9
10	0.6305	-0.5238	-0.5728	120.2
11	0.5949	-0.5378	0.5974	114.1
12	-0.0474	0.0027	0.9989	174.8
13	0.9957	0.0921	0.0021	90.6
14	0.6724	0.0339	0.7394	176.6
15	0.0479	0.0427	-0.9979	95.3
16	-0.6277	0.5786	0.5209	120.1
17	-0.5955	-0.5929	0.5421	113.7
18	0.0453	-0.999	0.0027	174.6
19	0.0503	-0.9977	-0.0446	84.7
20	0.0654	-0.7075	-0.7037	179.8
21	-0.0468	0.0524	0.9975	85
22	0.5618	0.6095	-0.5594	126.3
23	-0.5573	0.5597	-0.6134	126
24	-0.9979	-0.0452	-0.0473	179.7

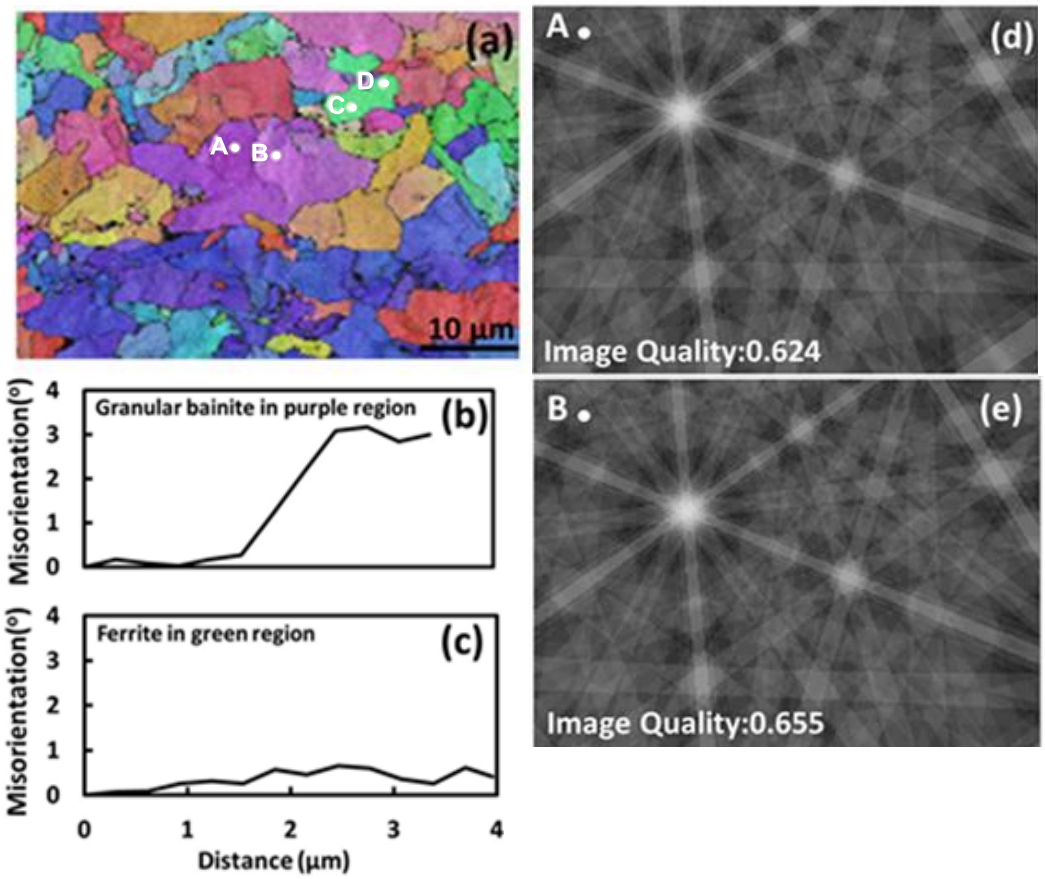

Figure 6. (a) EBSD map of Nb-450 Strip, (b) The variation of misorientation angle from point A to B in purple region, (c) The variation of misorientation angle from point C to D in green region, (d) and (e) the corresponding simulated Kikuchi patterns at points A and B in (a).

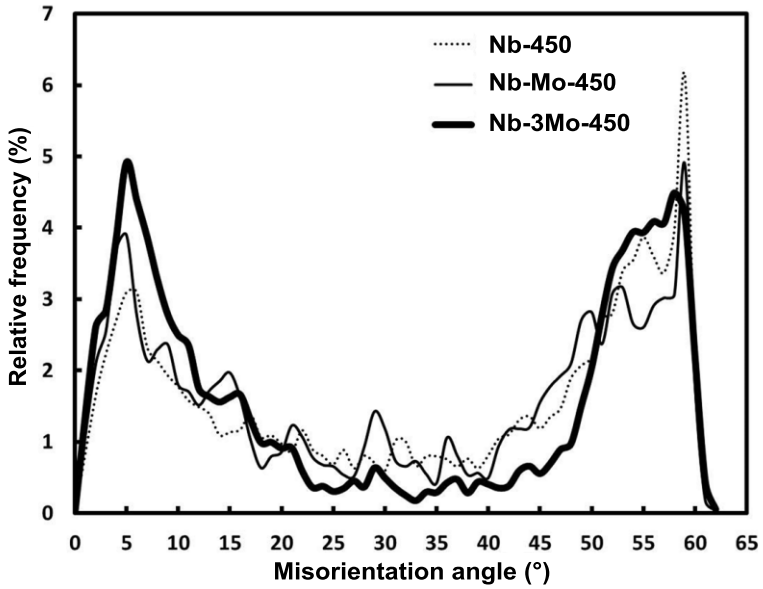

Figure 7. The misorientation angle profiles for Steels Nb-450, Nb-Mo-450 and Nb-3Mo-450.

In this work, the tempered bainite in the strip samples has been studied using Vickers hardness measurements and HRTEM examination. Vickers hardness measurement for granular bainite was performed under a load of 1 kg in order to indent on the granular bainite only. Each data point of Vickers hardness (with the standard deviation of about HV 5 – 8) was obtained from 30 measurements on granular bainite areas on each sample. Figure 8 shows the Vickers hardness data for strip samples Nb-450, Nb-Mo-450 and Nb-3Mo-450 after tempering at 600 ºC for different time intervals, ranging from 0.5 to 8 hours. It is clearly indicated that tempering steels Nb-450, Nb-Mo-450 and Nb-3Mo-450 does not cause a decrease in hardness after low tempering times; this behavior is obviously different from that of tempering martensite. For martensite, secondary hardening definitely involves the replacement of metastable cementite with the alloy carbides. The formation of these alloy carbides requires the long-range diffusion of the corresponding substitutional atoms and their precipitation is rather sluggish. It has been generally recognized that secondary hardening reactions in alloy steels with a bainitic microstructure are slower than with martensite because the coarser cementite particles in bainite take a longer time to dissolve before alloy carbides form [15]. However, in the present work, the experimental steels have an extremely low C concentration (0.05 wt.%C) in order to reduce or eliminate the interplate cementite in the bainitic ferrite matrix; interference from cementite during tempering can be surely avoided. It is worth noting that during the course of tempering at 600 ºC the hardness of sample Nb-3Mo increased to its highest value, HV 245, (by an increment of HV 20) after the 1 hour tempering treatment and the hardness is maintained at the same high level even after 8 hours. The hardness of samples Nb-Mo and Nb-450 showed similar trends, rising to the peak values, HV 233 (by an increment of HV 18) and HV 228 (by an increment of HV 20), respectively, after a 1 hour tempering time; after the peaks, their hardness declined sluggishly and decreased only by a small amount even after an 8 hour tempering time. It is evident that the Nb and Nb-Mo containing low-C bainitic steel strips have the advantage of obtaining secondary hardening at a 600 ºC tempering temperature.

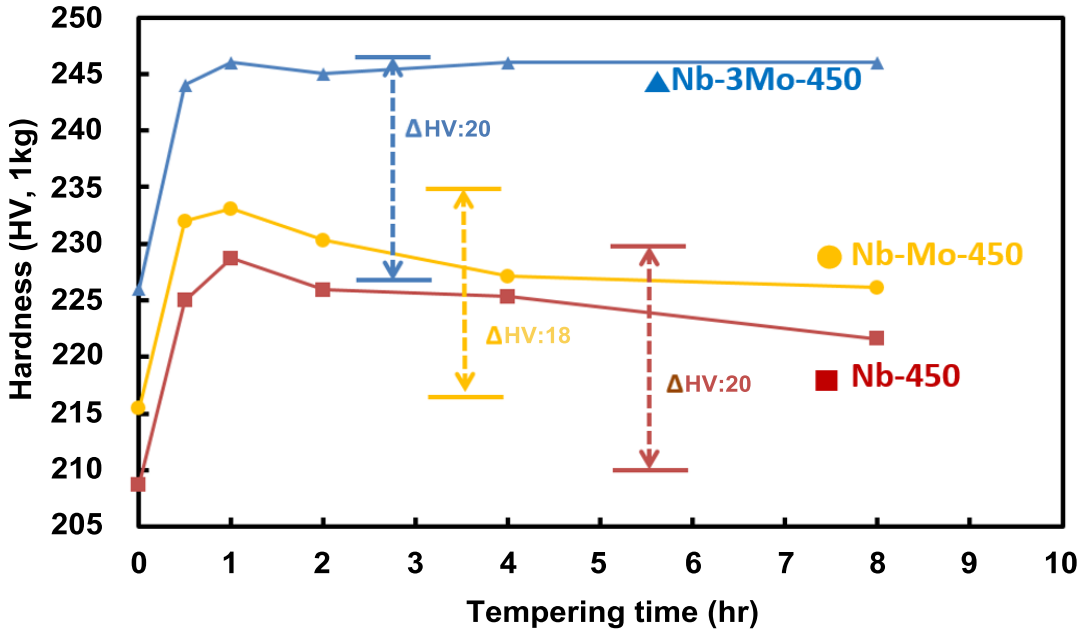

Figure 8. Hardness of granular bainite vs. tempering time at 600 ºC.

During the hot deformation of the prior austenite, the strain-induced Nb carbides precipitate and possess a cube-cube orientation relationship with the prior austenite [18]. In the course of cooling to room temperature, the deformed austenite transforms to allotriomorphic ferrite and bainite. The strain-induced Nb carbides usually have a size of more than 20 nm [19] and they possess no particular orientation relationship with the allotriomorphic ferrite [20], but adopt a Kurdjumov-Sachs (K-S) orientation relationship with bainite [19]. In contrast, during the tempering of bainite, nanometer-sized Nb carbides precipitate and have a Baker-Nutting orientation relationship with the tempered bainite [21-23]. Thus, the difference in orientation relationships can be utilized to identify the Nb carbides formed in the tempered bainite. TEM micrographs in Figure 9 display the tempered granular bainite in steel Nb-450 after tempering at 600 ºC for 1 hour; they show that nanometer-sized Nb carbides preferentially precipitated at dislocation lines. It is reasonably assumed that Nb atoms, a strong carbide-forming element, would diffuse toward the dislocation line and associate with C to precipitate MC-type carbides to reduce the lattice strain [24]. It is clear that granular bainite exhibits a significant secondary hardening effect by precipitating nanometer-sized carbides at dense dislocation lines. However, the addition of Mo raises the hardness of granular bainite in steels Nb-Mo-450 and Nb-3Mo-450 (as shown in Figure 8). As the secondary hardening is associated with alloy-carbide forming, it is vital to reveal the detail of the nanometer-sized carbides evolution in low-C bainite during the course of tempering. In previous conventional TEM research work for tempered bainite in low-C Nb and Nb-Mo containing steels [21-23], the Baker-Nutting (B-N) orientation relationship for carbide/ferrite matrix has been reported. However, the HRTEM image with its corresponding FFT (Fast Fourier Transformation) diffractogram provides a unique way for investigation of the nano-sized carbide/ferrite orientation [25]. In the present work, it has been confirmed that during tempering, extremely small nano-sized carbides are formed and these carbides satisfy the B-N orientation relationship with the bainitic ferrite matrix, $(0\ 0\ 1)_{carbide}//(0\ 0\ 1)_{\alpha}$ and $[\bar{1}\ 1\ 0]_{carbide}//[1\ 0\ 0]_{\alpha}$. In the habit plane of carbides on $(0\ 0\ 1)_{carbide}$, the lattice mismatch is extremely small: $[d_{(0\ 1\ 1)carbide} - d_{(0\ 1\ 0)\alpha}] / d_{(0\ 1\ 0)\alpha} = (0.313 - 0.2866) / 0.2866 = 0.093$, whereas perpendicular to the habit plane, the lattice mismatch is relatively large: $[d_{(0\ 0\ 2)carbide} - d_{(0\ 0\ 1)\alpha}] / d_{(0\ 0\ 1)\alpha} = (0.443/2 - 0.2866) / 0.2866 = -0.227$. Therefore, such lattice mismatches favor the formation of thin platelets. It is probable that carbides nucleate as spherical particles to maintain the minimum interface energy with the ferrite matrix in the early stages, and then grow rapidly in the best matched direction in a plate-like form during tempering, as shown in Figures 9 and 10. When the zone axis $[\bar{1}\ 1\ 0]_{carbide}//[1\ 0\ 0]_{\alpha}$ is chosen for HRTEM observation, the habit plane $(0\ 0\ 2)_{carbide}//(0\ 0\ 2)_{\alpha}$ presents an edge-on configuration to the incident beam direction, as shown in Figures 8 and 9.

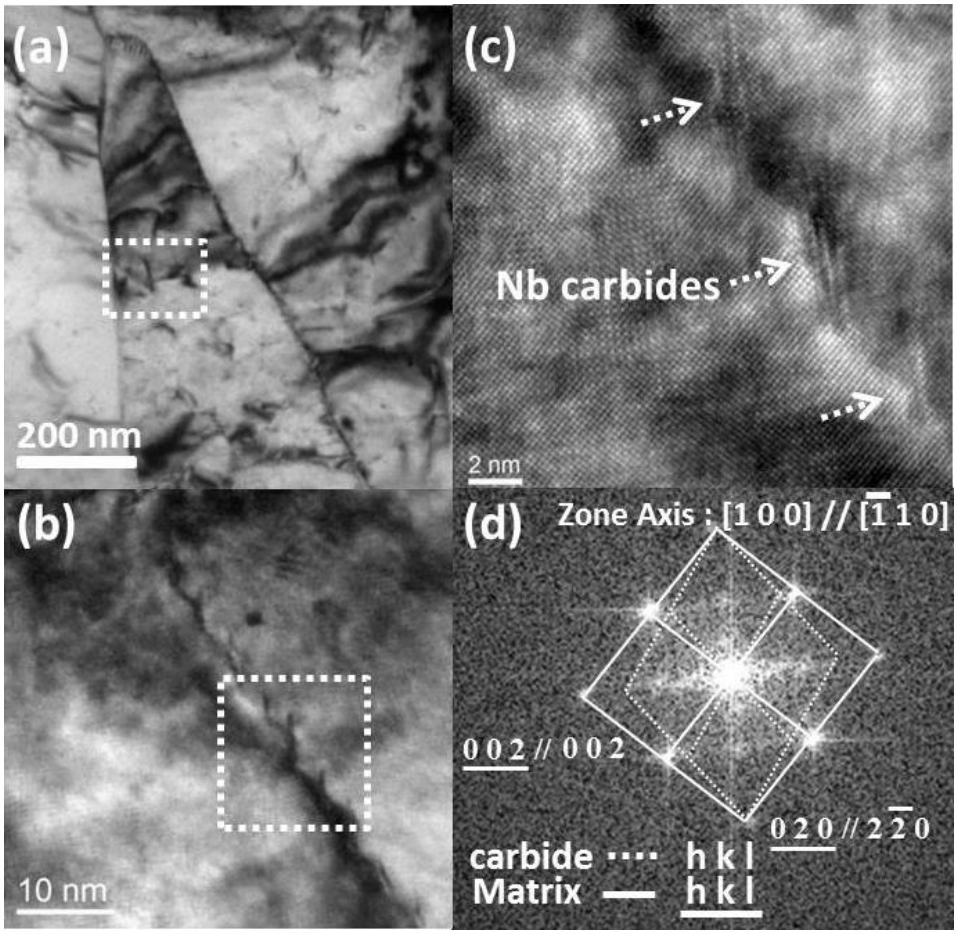

Figure 9. (a) Substructure of tempered granular bainite in Steel Nb-450 after tempering at 600 ºC for 1 hour, (b) the distribution of nanometer-sized carbides located at the dislocation line in the enlarged region of (a) with dashed white frame, (c) the detailed morphology of nanometer-sized carbides in the enlarged region of (b) with dashed white frame, (d) corresponding FFT image of carbides and bainitic matrix in (c).

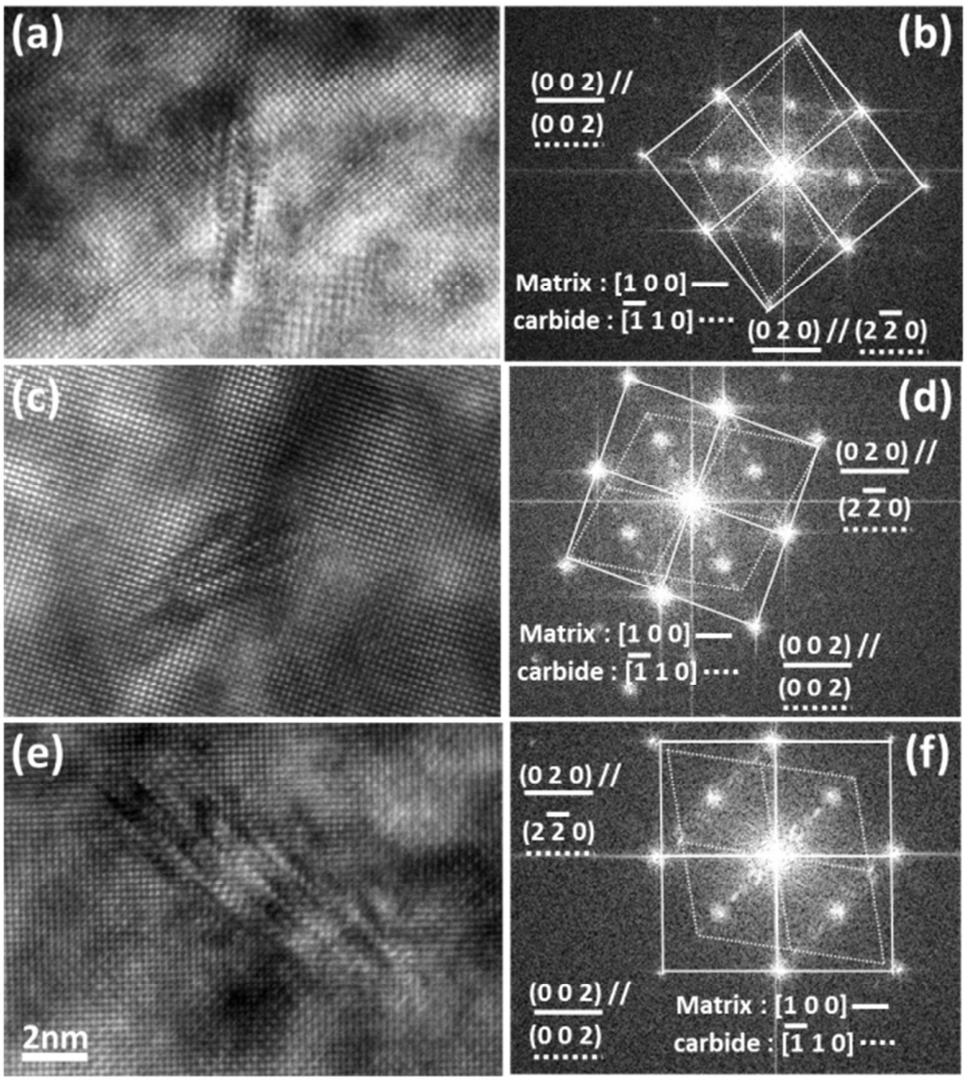

Figure 10. HRTEM images illustrating the nanometer-sized carbides in bainitic matrix of; (a) Nb-strip, (c) Nb-Mo strip, and (e) Nb-3Mo strip after 1 hour tempering; (b), (d) and (f) are the corresponding FFT images.

The effect of Mo addition on the size of Nb carbides can be clarified by evaluating variations in the length of carbides with tempering as shown in Figure 11. Each data point of average carbide length and Mo/Nb atomic ratio was estimated by 50 and 20 measurements respectively, on nanometer-sized carbides. For the samples tempered at 600 °C for 1 hour, average lengths of carbide in strip samples Nb-450, Nb-Mo-450 and Nb-3Mo-450 were respectively 3.7±1.1 nm, 3.8±0.6 nm, and 4.4±1.6 nm. For the samples tempered at 600 °C for 8 hours, average lengths of carbide in strip samples Nb, Nb-Mo and Nb-3Mo were respectively 4.3±0.8 nm, 4.3±1.3 nm and 5.5±2.1 nm.

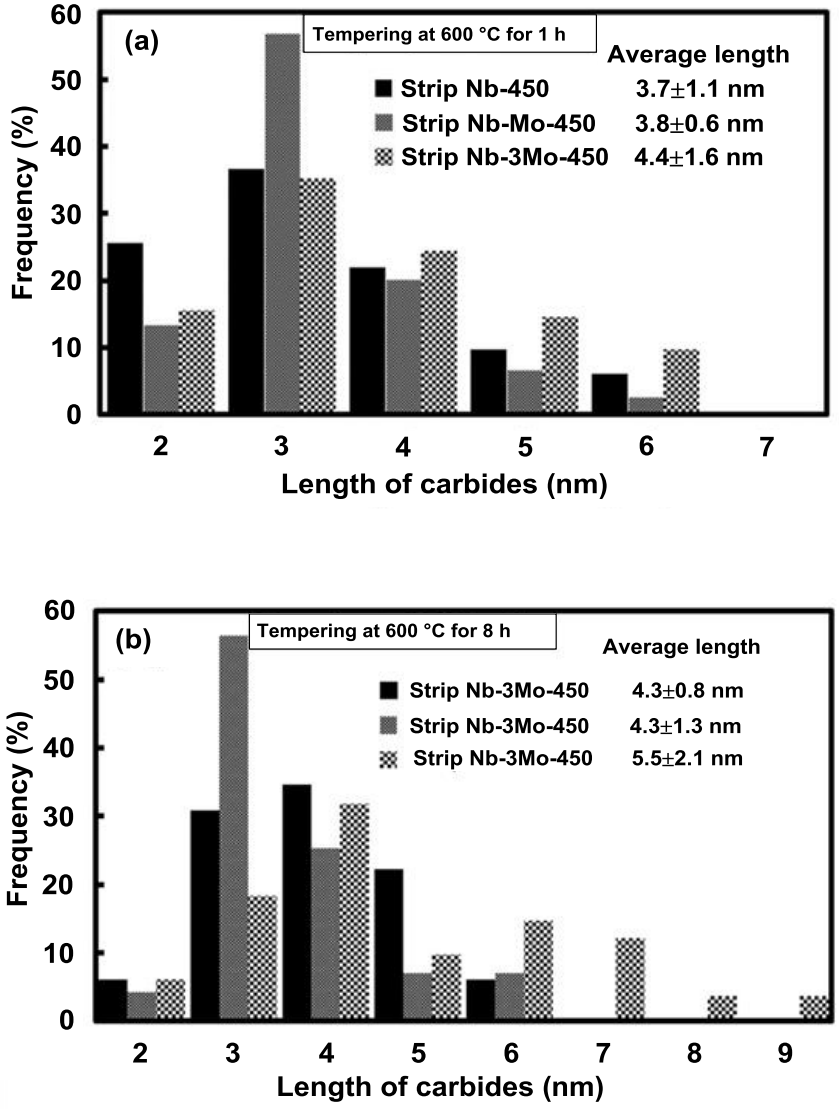

Figure 11. The distribution of nanometer-sized carbides in length in all three steels after; (a) 1 hour of tempering and (b) 8 hours of tempering.

It is worth noting that the addition of Mo did not have a significant effect on the size of nanometer-size carbides formed in the tempered granular bainite structures investigated. The degree of incorporated Mo atoms in Nb carbides has been simultaneously assessed by nano-probe EDX spectroscopy. The spectra in Figures 12(a) and (b) were obtained from strip sample Nb-Mo tempered at 600 °C for 1 and 8 hours respectively; the atomic ratio Nb/Mo for the former was 4.87 and the latter 4.07. The spectra in Figures 11(c) and (d) were obtained from sample Nb-3Mo tempered at 600 °C for 1 and 8 hours respectively; the atomic ratio Nb/Mo for the former was 1.12 and the latter 1.10. Mo plainly becomes a dominant carbide forming element in (Nb_xMo_{1-x}) carbides with increasing Mo addition, which is consistent with thermodynamic calculations in previous research [26].

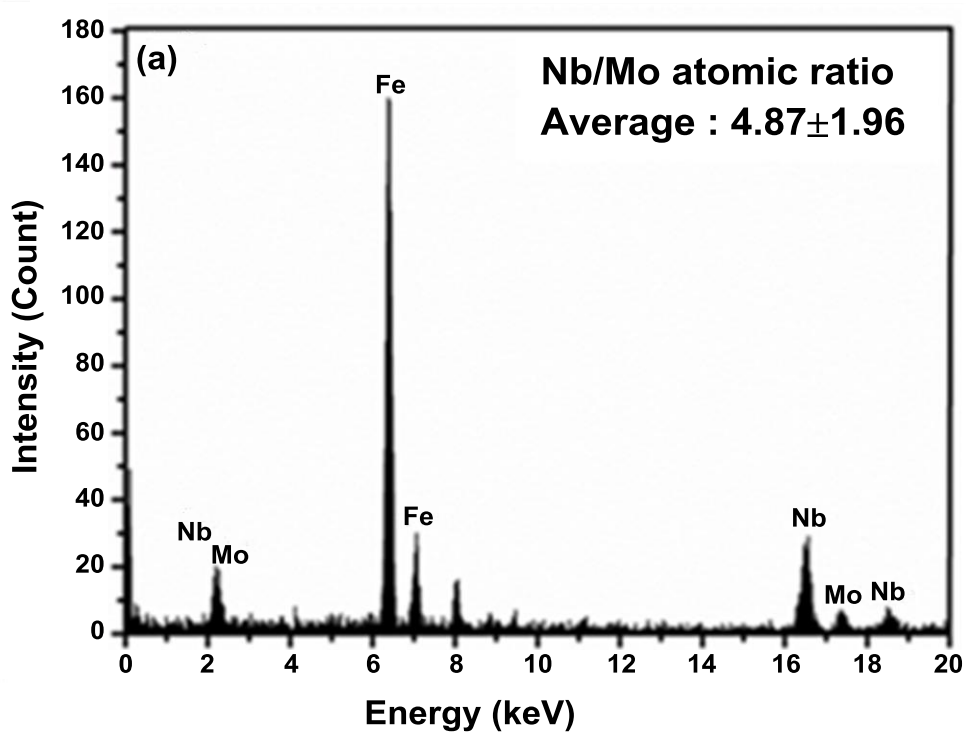
(a)
Nb/Mo atomic ratio
Average : 4.87±1.96
Fe
Fe
Nb
Mo
Nb
Mo
Nb
Intensity (Count)
Energy (keV)
0
20
40
60
80
100
120
140
160
180
0
2
4
6
8
10
12
14
16
18
20

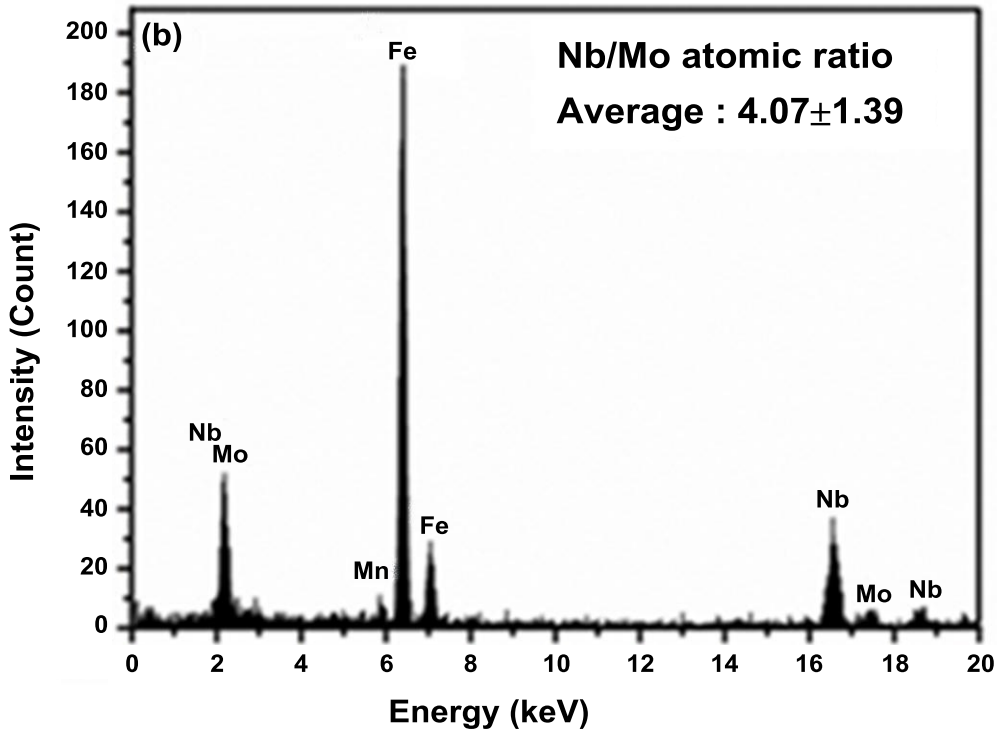
(b)
Nb/Mo atomic ratio
Average : 4.07±1.39
Fe
Nb
Mo
Mn
Fe
Nb
Mo
Nb
Intensity (Count)
Energy (keV)
0
20
40
60
80
100
120
140
160
180
200
0
2
4
6
8
10
12
14
16
18
20

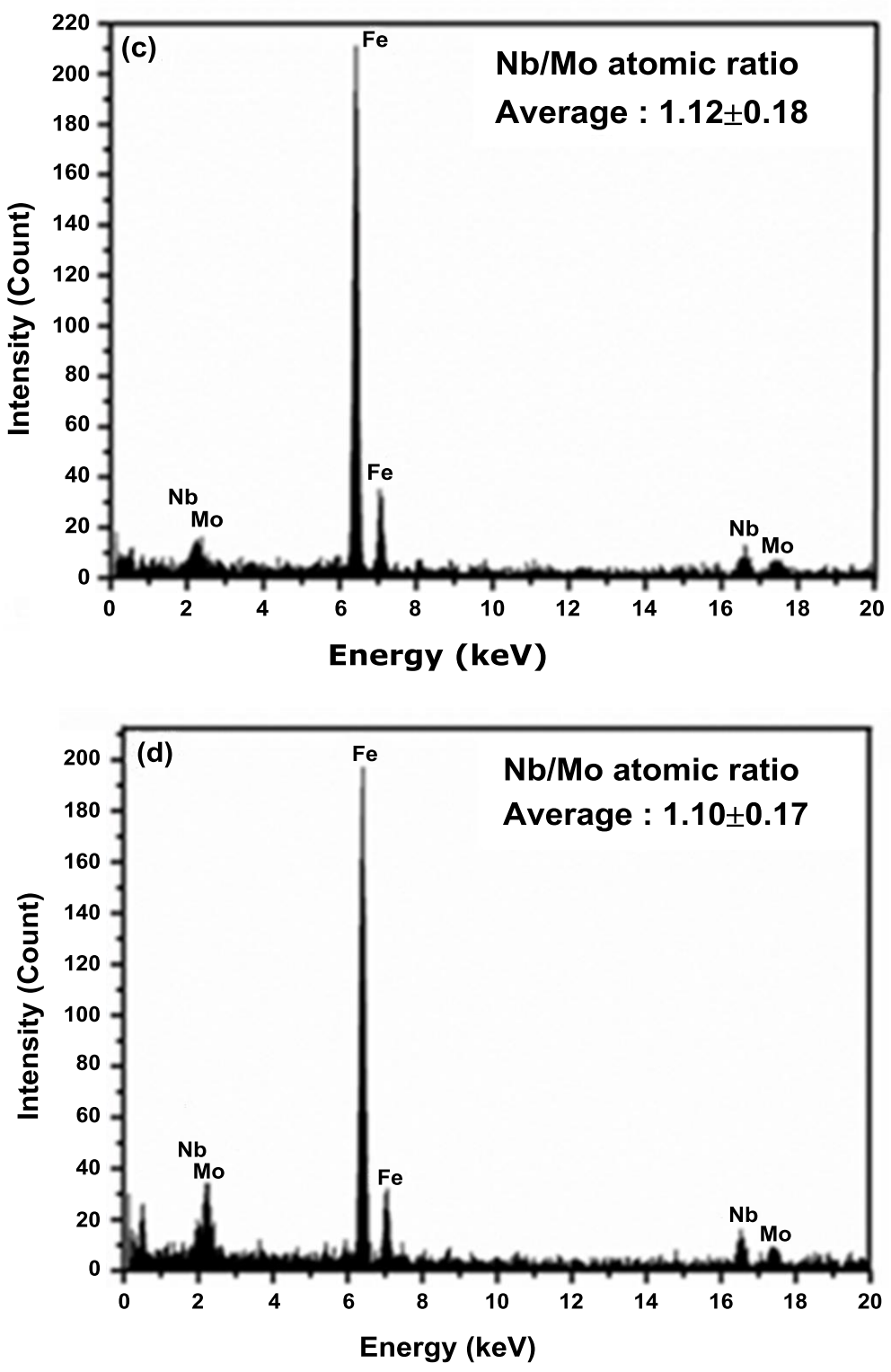

Figure 12. EDX spectra in (a) and (b) obtained from steel Nb-Mo tempered at 600 °C for 1 and 8 hours, respectively; the spectra (c) and (d) obtained from steel Nb-3Mo tempered at 600 °C for 1 and 8 hours, separately.

In this work, the granular bainite in the bainitic steel strips possessed a high dislocation density of about 5.3×10^{14} m^{-2} − 5.6×10^{14} m^{-2}. The detailed method for dislocation density measurement has been described elsewhere [27]. The dislocations are apparently stable at high temperatures; the dislocation density does not change significantly during tempering at 600 °C as seen in Table IV, which indicates that the dislocation densities of the tempered samples Nb-450, Nb-Mo-450 and Nb-3Mo-450 had only reduced to the range of 3.6×10^{14} m^{-2} − 4.9×10^{14} m^{-2}. It is obvious that the dislocations in the Nb and Nb-Mo bearing steels investigated in this work possessed a remarkable thermal stability during tempering at 600 °C.

Table IV. The Dislocation Density (m^{-2}) of Granular Bainite in the Three Steels after Tempering at 600 °C for 0, 1 and 8 hours

Time/hours	Nb-450	Nb-Mo-450	Nb-3Mo-450
0	(5.3±1.2) x10^{14}	(5.4±0.9) x10^{14}	(5.6±0.8) x10^{14}
1	(4.6±0.8) x10^{14}	(4.8±1.2) x10^{14}	(4.9±1.0) x10^{14}
8	(3.9±1.3) x10^{14}	(3.9±1.4) x10^{14}	(3.6±1.1) x10^{14}

The mechanical properties for the strip samples are presented in Tables V and VI. The data clearly shows that steel Nb-3Mo possessed the optimum combination of strength and elongation after tempering at 600 °C for 1 hour. Steel Nb-3Mo with the addition of 0.3 wt.%Mo had the advantage of producing a high volume fraction of granular bainite, which gained significant benefits from secondary hardening. It can be concluded that during tempering, the amount of nanometer-sized carbides increases in bainitic strip steels with a higher level of Mo content, since the number of alloy carbides formed in the granular bainite is proportional to the volume fraction of granular bainite.

Table V. The Yield/Tensile Strength Values(MPa) of the Three Steels after Tempering at 600 °C for 0, 1 and 8 hours

Time/hours	Nb-450	Nb-Mo-450	Nb-3Mo-450
0	512/630	479/683	575/679
1	594/652	619/678	672/718
8	586/638	605/655	651/702

Table VI. The Elongation (%) of the Three Steels after Tempering at 600 °C for 0, 1 and 8 hours

Time/hours	Nb-450	Nb-Mo-450	Nb-3Mo-450
0	22	21	19
1	29	27	27
8	30	27	27

Conclusions

In this work, three low-C Nb-containing strip steels with different levels of Mo (0, 0.1 and 0.3 wt.%) have been produced using a controlled-rolling and accelerated-cooling process. The findings can be summarized as follows:

1. All the steels contained large amounts of granular bainite. The substructure of granular bainite has been revealed by TEM; granular bainite is composed of parallel sub-unit ferrite platelets, with a thickness of about 0.5 μm. The parallel sub-unit ferrite platelets have a similar orientation and form a sheaf morphology, which is not different from ordinary bainite.

2. SEM-EBSD techniques have been utilized to obtain quantitative metallography data for the steels. The results clearly indicate that the addition of Mo promotes the formation of granular bainite.

3. The steel with the addition of 0.3 wt.%Mo had the advantage of producing a high volume fraction of granular bainite, and gained significant benefits from secondary hardening. Mo did not appear to further refine the (Nb,Mo) carbides but the increased proportion of the precipitate rich granular bainite led to increased strength whilst maintaining good ductility

Acknowledgement

This work was carried out with support from Companhia Brasileira de Metalurgia e Mineração (CBMM). The authors thank China Steel Corporation for providing the alloy steel strips.

References

1. H.K.D.H. Bhadeshia, Steel Technology International 1989, Ed. P. H. Scholes, (Sterling Publication International Ltd, 1989), 289-294.

2. T. Gladman, *The Physical Metallurgy of Microalloyed Steels*, (London, UK: The Institute of Materials, 1997).

3. N.K. Balliger and R.W.K. Honeycombe, "The Effect of Nitrogen on Precipitation and Transformation Kinetics in Vanadium Steels," *Metallurgical Transaction A*, 11 (1980), 420-430.

4. H.L. Andrade, M.G. Akben and J.J. Jonas, "Effect of Molybdenum, Niobium and Vanadium on Static Recovery and Recrystallisation on Solute Strengthening in Microalloyed Steels," *Metallurgical Transaction A*, 14 (1983), 1976-1984.

5. B. Dutta and C.M. Sellars, "Effect of Composition and Process Variables on Nb(C,N) Precipitation in Niobium Microalloyed Austenite," *Materials Science and Technology*, 3 (1987), 197-206.

6. C. Fossaert et al., "The Effect of Niobium on the Hardenability of Microalloyed Austenite," *Metallurgical and Materials Transactions A*, 26 (1995), 21-30.

7. M.G. Akben, B. Bacroix and J.J. Jonas, "Effect of Vanadium and Molybdenum Additions on High Temperature Recovery, Recrystallisation and Precipitation Behaviour of Niobium Based Microalloyed Steels," *Acta Metallurgica*, 31 (1983), 161-174.

8. M. Charleux et al., "Precipitation Behaviour and its Effect on Strengthening of an HSLA – Nb/Ti Steel," *Metallurgical and Materials Transactions A*, 32A (2001), 1635-1647.

9. S.C. Wang and J.R. Yang, "Effects of Chemical Composition, Rolling and Cooling Conditions on the Amount of Martensite/Austenite (M/A) Constituent Formation in Low Carbon Bainitic Steels," *Materials Science and Engineering A*, 154 (1992), 43-49.

10. S.C. Wang, R.I. Hsieh and J.R. Yang, "Effect of Rolling Processes on the Microstructure and Mechanical Properties of Ultralow Carbon Bainitic Steels," *Materials Science and Engineering A*, 157 (1992), 29-36.

11. J.R. Yang, C.Y. Huang and S.C. Wang, "The Development of Ultra Low Carbon Bainitic Steels," *Materials & Design*, 13 (1992), 335-338.

12. C.Y. Huang, J.R. Yang and S.C. Wang, "Effect of Compressive Deformation on the Transformation Behaviour of an Ultra Low Carbon Bainitic Steel," *Materials Transactions - The Japan Institute of Metals*, 34 (1993), 658-668.

13. J.R. Yang et al., "The Influence of Plastic Deformation and Cooling Rates on the Microstructural Constituents of an Ultra Low Carbon Bainitic Steel," *The Iron and Steel Institute of Japan International*, 35 (1995), 1013-1019.

14. C.S. Chiou, J.R. Yang and C.Y. Huang, "The Effect of Prior Compressive Deformation of Austenite on Toughness Property in an Ultra Low Carbon Bainitic Steel," *Materials, Chemistry and Phys*ics, 69 (2001), 113-124.

15. H.K.D.H. Bhadeshia, *Bainite in Steels*, 2nd edition, (London, UK: Iom Communications Ltd, 2001), 91-98.

16. H.K.D.H. Bhadeshia, *Worked Examples in the Geometry of Crystals*, (London, UK: Institute of Metals, 1987).

17. K.Y. Zhu et al., "An Approach to Define the Effective Lath Size Controlling Yield Strength of Bainite," *Materials Science and Engineering A*, 527 (2010), 6614-6619.

18. M. Enomoto, "Nucleation of Phase Transformations at Intragranular Inclusions in Steel," *Metals and Materials,* 4 (1998), 115-123.

19. W.B. Lee et al., "Carbide Precipitation and High Temperature Strength of Hot Rolled HSLA Steel," *Metallurgical and Materials Transactions A,* 33 (2002), 1689-1698.

20. F. Perrard et al., "TEM Study of NbC Heterogeneous Precipitation in Ferrite," *Philosophical Magazine,* 27 (2006), 4271-4284.

21. W.B. Lee et al., "Influence of Mo on Precipitation Hardening in Hot Rolled HSLA Steels Containing Nb," *Scripta Materialia,* 43 (2000), 319-324.

22. W.B. Lee et al., "Carbide Precipitation and High Temperature Strength of Hot Rolled High Strength, Low Alloy Steels Containing Nb and Mo," *Metallurgical and Materials Transactions A,* 33A (2002) 1689-1698.

23. K. Maruyama, K. Sawada and J. Koike, "Strengthening Mechanisms of Creep Resistant Tempered Martensitic Steel," *The Iron and Steel Institute of Japan International,* 41 (2001), 641-653.

24. H-J. Kestenbach, "Dispersion Hardening by Niobium Carbonitride Precipitation in Ferrite," *Journal of Materials Science and Technology,* 13 (1997), 731-739.

25. H.W. Yen et al., "Orientation Relationship Transition of Nanometer Sized Interphase Precipitated TiC Carbides in Ti Bearing Steel," *Journal* of *Materials Science and Technology,* 26 (2010), 421-430.

26. C.M. Enloe et al., "Compositional Evolution of Microalloy Carbonitrides in a Mo Bearing Microalloyed Steel," *Scripta Materilia,* 68 (2013), 55-58.

27. J.R. Yang and H.K.D.H. Bhadeshia, "The Dislocation Density of Acicular Ferrite in Steel Welds," *Welding Journal,* 69 (1990), 305-307.